Magnetic hysteresis up to 80 K in a dysprosium metallocene single-molecule magnet

Authors: Fu-Sheng Guo,[1] Benjamin M. Day,[1,2] Yan-Cong Chen,[3] Ming-Liang Tong[3], Akseli Mansikkamäki[4], Richard A. Layfield[1]*.

Affiliations:

[1]Department of Chemistry, School of Life Sciences, University of Sussex, Falmer, BN1 9QJ, U.K.

[2]School of Chemistry, The University of Manchester, Oxford Road, Manchester, M13 9PL, U.K.

[3]Key Laboratory of Bioinorganic and Synthetic Chemistry of the Ministry of Education, School of Chemistry, Sun-Yat Sen University, Guangzhou 510275, P.R. China.

[4]Department of Chemistry, Nanoscience Centre, University of Jyväskylä, P. O. Box 35, FI-40014 Jyväskylä, Finland.

*Correspondence to: R.Layfield@sussex.ac.uk.

Abstract: Single-molecule magnets (SMMs) containing only one metal center may represent the lower size limit for molecule-based magnetic information storage materials. Their current drawback is that all SMMs require liquid-helium cooling to show magnetic memory effects. We now report a chemical strategy to access the dysprosium metallocene cation $[(Cp^{iPr5})Dy(Cp^*)]^+$ (Cp^{iPr5} = penta-iso-propylcyclopentadienyl, Cp***** = pentamethylcyclopentadienyl), which displays magnetic hysteresis above liquid-nitrogen temperatures. An effective energy barrier to reversal of the magnetization of U_{eff} = 1,541 cm^{-1} is also measured. The magnetic blocking temperature of T_B = 80 K for this cation overcomes an essential barrier towards the development of nanomagnet devices that function at practical temperatures.

One Sentence Summary: Magnetic blocking above liquid-nitrogen temperatures is demonstrated in a dysprosium single-molecule magnet.

Main Text:

The observation of slow magnetic relaxation in coordination compounds that contain a single lanthanide ion stimulated considerable interest in monometallic single-molecule magnets (SMMs) (*1*). This family of materials shiws magnetic hysteresis properties that arise from the electronic structure at the molecular level rather than interactions across comparatively large magnetic domains (*2-4*). In addition to the considerable fundamental interest in SMMs and related magnetic molecules, their magnetic memory properties have inspired proposals for applications as spin qubits (*5*) and in nanoscale spintronic devices (*6*). A key performance parameter of an SMM is the magnetic blocking temperature, T_B, one description of which refers the maximum temperature at which it is possible to observe hysteresis in the field-dependence of the magnetization, subject to the field sweep rate. The blocking temperature provides a means of comparing different SMMs and, to date, the vast majority that show any hysteresis at all require liquid-helium cooling to do so (*7,8*). A few notable examples have emerged from the extreme cold to set record blocking temperatures above the liquid-helium regime (*9-12*), including the dysprosium metallocene $[(Cp^{ttt})_2Dy][B(C_6F_5)_4]$ (Cp^{ttt} = 1,2,4-tri-*tert*-butylcyclopentadienyl), which showed magnetic hysteresis with coercivity up to 60 K (*13-15*); however, this threshold still falls markedly short of the more practically accessible 77 K temperature at which nitrogen liquefies. We now show that

by designing the ligand framework so that two key structural parameters – i.e. the Dy-Cp_{cent} distances (cent refers to the centroid of the Cp ligand) and the Cp-Dy-Cp bending angle – are rendered short and wide, respectively, we achieve an axial crystal field of sufficient strength to furnish an SMM that shows hysteresis above 77 K.

A dysprosium metallocene cation was targeted with cyclopentadienyl substituents of sufficient bulk to produce a wide Cp-Dy-Cp angle, but not too bulky to preclude close approach of the ligands. Thus, the borohydride precursor complex [(η^5- Cp^{iPr5})Dy(η^5-Cp^*)(BH_4)] (**2**) (Cp^{iPr5} = penta-iso-propylcyclopentadienyl, Cp^* = pentamethylcyclopentadienyl) was synthesized by treating [Dy(η^5-Cp^{iPr5})(BH_4)$_2$(THF)] (**1**) with KCp^* (Fig. 1). The molecular structures of **1** and **2** were determined by x-ray crystallography (tables S1-S3, figs S4, S5). The target compound [(η^5-Cp^*)Dy(η^5-Cp^{iPr5})][$B(C_6F_5)_4$] (**3**), hereafter abbreviated [Dy-5*][$B(C_6F_5)_4$], was then isolated in 60% yield by treating **2** with the super-electrophile [$(Et_3Si)_2(\mu$-H][$B(C_6F_5)_4$] (*16*). An x-ray crystallographic analysis of the molecular structure of **3** at 150 K (fig. 1, figs S6-S7, tables S1, S4) revealed that the Dy-5* cation features Dy-Cp^* and Dy-Cp^{iPr5} distances of 2.296(1) Å and 2.284(1) Å, respectively, which are, on average, 0.026 Å shorter than the analogous distances of 2.32380(8) Å and 2.30923(8) Å determined for $[(Cp^{ttt})_2Dy]^+$ (*13*). Furthermore, the Cp-Dy-Cp angle in Dy-5* is 162.507(1)°, and hence almost 9.7° wider than the angle of 152.845(2)° found in $[(Cp^{ttt})_2Dy]^+$. Based on these structural parameters, the crystal field in Dy-5* should be stronger and more axial than in $[(Cp^{ttt})_2Dy]^+$, and hence an improvement in the SMM properties can be expected.

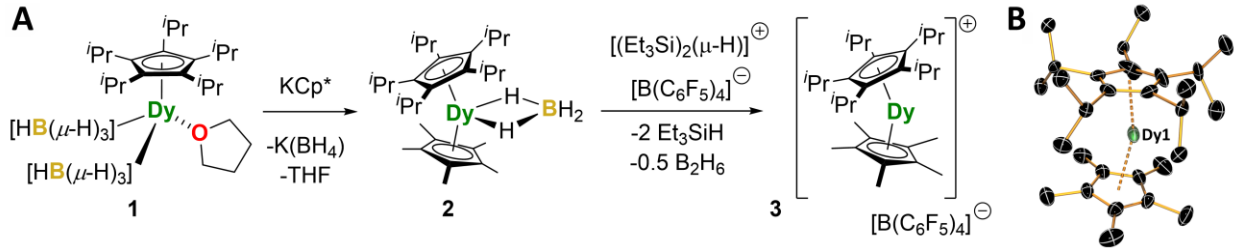

Fig. 1. Synthesis and molecular structures. (**A**) Reaction scheme for the synthesis of **3**. Cp^* = pentamethylcyclopentadienyl (**B**) Thermal ellipsoid representation (50% probability) of the molecular structure of the Dy-5* cation in **3**, as determined by x-ray crystallography (for clarity, the hydrogen atoms and $[B(C_6F_5)_4]^-$ counter anion are omitted).

The D.C. molar magnetic susceptibility (χ_M) was measured for compounds **1-3** in the temperature range 2 to 300 K using an applied field of 1000 Oe, and the field-dependence of the magnetization for **1** and **2** was measured at T = 2 and 5 K using fields up to 70 kOe (figs S8-S12). A description of the properties of **1** and **2** is provided in the Supplementary Materials. For **3**, the $\chi_M T$ value was measured to be 13.75 cm^3 K mol^{-1} at 300 K and then manifested a steady decrease down to 75 K. At lower temperatures a sharp drop in $\chi_M T$ was observed, indicating the onset of magnetic blocking, with a value of 0.94 cm^3 K mol^{-1} reached at 2 K. Overall, the D.C. magnetic properties of compounds **1-3** are typical for a monometallic complex of Dy^{3+} with a $^6H_{15/2}$ ground multiplet (*17*). The SMM properties of compounds **1-3** were then established through measurements of the in-phase (the real component, χ') and the out-of-phase (the imaginary component, χ'') A.C. susceptibilities as functions of the A.C. frequency (ν) and temperature, using an oscillating field of 5 Oe and zero applied D.C. field (figs S13-S28, tables S5-S7). Focusing again on **3**, the $\chi''(\nu)$ isotherms show well-defined maxima up to 130 K (Fig. 2). The $\chi'(\nu)$ and $\chi''(\nu)$ data were then used to derive Cole-Cole plots of $\chi''(\chi')$ for relaxation in the temperature

range 82 to 138 K in intervals of 2 K, with each plot adopting a parabolic shape (figs S26-S28,). Accurate fits of the A.C. susceptibility plots were obtained using equations describing χ' and χ'' in terms of frequency, the isothermal susceptibility (χ_T), adiabatic susceptibility (χ_S), the relaxation time (τ), and the fitting parameter α to represent the distribution of relaxation times (eq S1, S2) (*18*).

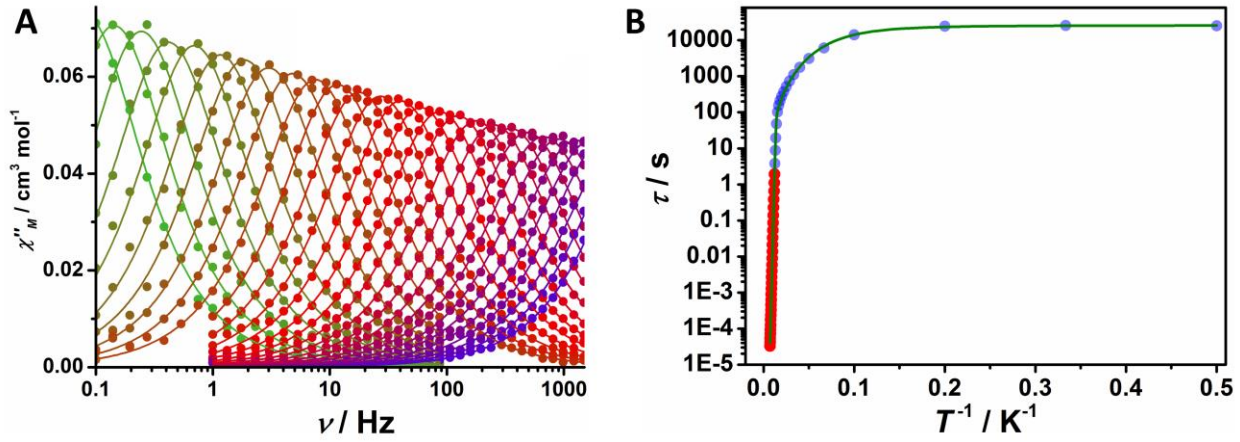

Fig. 2. Dynamic magnetic properties. (**A**) Frequency dependence of the out-of-phase χ''_M molar magnetic susceptibility for **3**, collected in zero D.C. field at A.C. frequencies of ν = 0.1 to 1488 Hz from 82 K (green trace) to 138 K (purple trace) in 2 K intervals. Solid lines represent fits to the data using equations S1 and S2, with R^2 = 0.99823-0.99988. (**B**) Temperature dependence of the relaxation time for **3**. The red points are from the A.C. susceptibility data and the blue points are from measurements of the D.C. magnetic relaxation time. The solid green line is the best fit to $\tau^{-1} = \tau_0^{-1}e^{-U_{\mathrm{eff}}/k_{\mathrm{B}}T} + CT^n + \tau_{QTM}^{-1}$, using the parameters stated in the text.

The resulting values of α = 0 to 0.027 indicate a very narrow range of relaxation times in the high-temperature regime. The relaxation times at temperatures in the range 2 to 83 K were determined in intervals of approximately 5 K from plots of the magnetization decay *vs.* time (figs S29-S48, table S8). These data show, for example, that the magnetization in **3** decays almost to zero over a 50-second time period at 77 K, increasing to approximately 500 minutes at 15 K. The temperature at which τ = 100 s is 66 K. The relaxation times determined from the A.C. and D.C. measurements were then combined to obtain further insight into the magnetic relaxation by plotting τ as a function of T^{-1} (fig. 2), which revealed a strong, linear dependence of the relaxation time on temperature in the range 55 to 138 K. The $\tau(T^{-1})$ plot in the range 10 to 55 K is curved in nature and represents an intermediate regime before purely temperature-independent relaxation is observed below 10 K. The relaxation time can be expressed as $\tau^{-1} = \tau_0^{-1}e^{-U_{\mathrm{eff}}/k_{\mathrm{B}}T} + CT^n + \tau_{QTM}^{-1}$, in which the first term represents Orbach relaxation with U_{eff} as the effective energy barrier to relaxation of the magnetization, the second term represents the contribution from Raman processes, and the third term represents the rate of quantum tunneling of the magnetization. Using this equation, an excellent fit (R^2 = 0.99958) of the data was obtained with τ_0 = 4.2(6) × 10^{-12} s, U_{eff} = 1,541(11) cm^{-1}, C = 3.1(1) × 10^{-8} s^{-1} K^{-n} and n = 3.0(1), and τ_{QTM} = 2.5(2) × 10^4 s. The U_{eff} value determined for **3** exceeds the value of 1,277 cm^{-1} determined for [(Cp^{ttt})$_2$Dy][B(C_6F_5)$_4$] by approximately 20% (*13*).

Potential applications of SMMs in information storage devices rely on the occurrence of magnetic remanence and coercivity: therefore, the hysteresis is a critical consideration (*19*). For **3**, using a relatively fast field sweep rate of 200 Oe s^{-1} revealed $M(H)$ hysteresis from 2 K up to 85 K, with the loops gradually closing as the temperature increased (Figs 3A, 3B). At these temperature limits, coercive fields of 50 kOe and 210 Oe (5.0 T and 21 mT), respectively, were measured (Fig. 3C, fig. S49, table S9). Fixing the temperature at 77 K, a reduction in the sweep rate resulted in the coercive field approximately halving with the rate, i.e. H_c = 5,802 Oe at 700 Oe s^{-1}, 2,946 Oe at 350 Oe s^{-1}, 1,688 Oe at 200 Oe s^{-1}, 825 Oe at 100 Oe s^{-1}, 398 Oe at 50 Oe s^{-1} and 191 Oe at 25 Oe s^{-1} (fig. S50, table S10). The observation of coercivity in **3** at 25 Oe s^{-1} is significant because this sweep rate is slower than the 39 Oe s^{-1} used to determine the blocking temperature of 60 K for $[(Cp^{ttt})_2Dy][B(C_6F_5)_4]$ (*13*). At 80 K and 25 Oe s^{-1}, a coercive field of 63 Oe was measured (Fig. 3D), and the loops were completely closed at higher temperatures. Consistent with this finding, the field-cooled and zero-field-cooled magnetic susceptibilities for **3** diverged at 78 K (fig. S51). By analogy with the development of high-T_C superconductors, we propose to designate the Dy-5^* cation in **3** as a high-temperature, or high-T_B, single-molecule magnet.

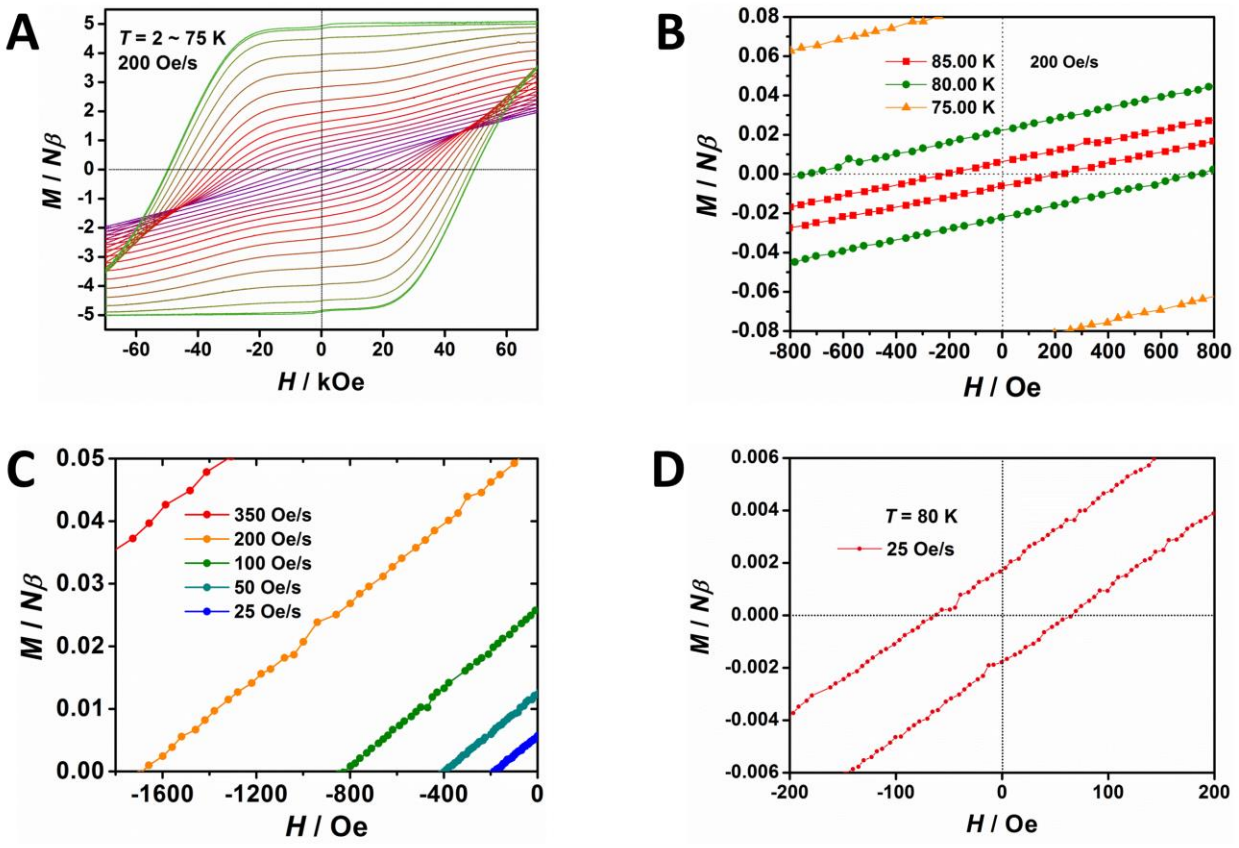

Fig. 3. Magnetic hysteresis properties of 3. Magnetization vs. field hysteresis loops in the temperature ranges of (**A**) 2 to 75 K and (**B**) 75 to 85 K using a field sweep rate of 200 Oe s^{-1}. (**C**) Expansion of the hysteresis loops at 77 K showing the coercive fields. (**D**) Hysteresis loops at 80 K using a field sweep rate of 25 Oe s^{-1}.

The importance of the strong axial crystal field in the Dy-5* cation combined with the absence of an equatorial field is illustrated further by comparing the U_{eff} and T_B values for **3** with those of the precursors **1** and **2**. In the case of **1**, the Cp^{iPr5} ligand provides a strong axial field, but the pseudo-octahedral coordination geometry introduces a non-negligible equatorial field and, whilst slow magnetic relaxation in zero field is observed with this system, the position of the maxima in $\chi''(\nu)$ are temperature-independent up to 10 K and only observed up to 30 K (figs S13-S16). The resulting energy barrier of 241(7) cm^{-1} is comparatively small, and the rate of quantum tunnelling of the magnetization (QTM) is, at 5.0(1) × 10^{-3} s (fig. S17), some seven orders of magnitude faster than found with **3**. The competing equatorial field in **2** is more prominent as the maxima in $\chi''(\nu)$ are very weakly temperature-dependent from 3 to 20 K, with the resulting energy barrier a negligible 7(1) cm^{-1} (figs S19-S22). In both **1** and **2**, the $M(H)$ hysteresis loops collected at 2 K and 200 Oe s^{-1} are waist-restricted, with no coercivity and only small openings as the field magnitude increases (figs S18, S23).

Ab initio calculations have enabled quantitative analysis of the properties of SMMs on a microscopic scale (*20*), particularly systems with η^n-bonded organometallic ligands (*21-30*). Calculations on the Dy-5* cation were performed at the XMS-CASPT2//SA-CASSCF/RASSI level (*31, 32*): the resulting energies, principal components of the ***g***-tensors and the principal magnetic axes of the eight lowest Kramers' doublets in Dy-5* corresponding to the CF-split states of the $^6H_{15/2}$ ground multiplet are listed in table S11. The principal magnetic axis in the ground doublet of Dy-5* (Fig. 4) is projected towards the centroids of the two cyclopentadienyl ligands, with the principal axes of the next six doublets almost collinear and the largest deviation angle 5.3° with the fifth doublet. The highest doublet is perpendicular to the ground doublet.

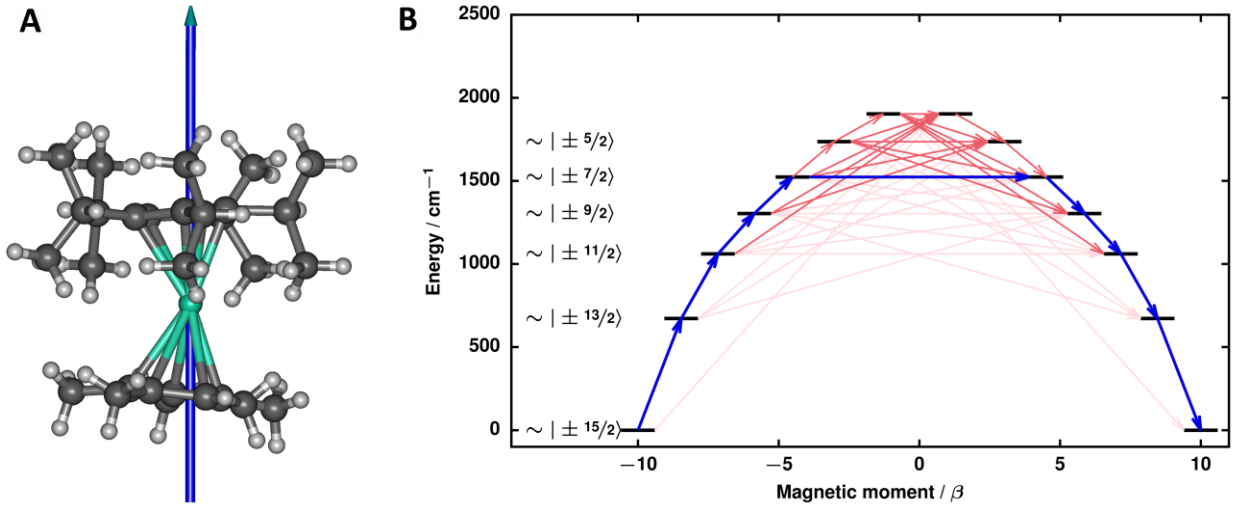

Fig. 4. Magnetic relaxation in the Dy-5* cation. (**A**) The principal magnetic axis of the ground Kramers' doublet. (**B**) Relaxation mechanism for Dy-5*. Blue arrows show the most probable relaxation route and red arrows show transitions between states with less probable but non-negligible matrix elements: darker shading indicates a higher probability.

The ***g***-tensor of the ground doublet is calculated to be perfectly axial, i.e. $g_x = g_y = 0.000$ and $g_z = 20.000$ (table S11), which is consistent with the experimental hysteresis measurements in which QTM is completely blocked at zero field. In the six lowest doublets, the CF is highly axial and each state can be assigned to a definite projection (greater than 96% character) of the total angular

momentum, M_J (table S12). The transverse components of the ***g***-tensors increase roughly by an order of magnitude in each doublet upon moving to higher energy. In the fifth doublet the transverse components start to become significant and in the sixth doublet the transverse components are large enough to allow considerable tunneling. In the two highest states, the axiality is weaker and considerable mixing occurs under the CF, which most likely results from the asymmetry of the coordination environment.

The *ab-initio* CF parameters were calculated for the Dy-5* cation following a previously established methodology (*33, 34*) and are listed in table S13. The off-diagonal elements of the CF operator clearly have non-negligible elements due to the low C_1 point symmetry of Dy-5*, however the axial second-rank parameter B_2^0 is at least two orders of magnitude larger than any other parameter. This creates a highly axial CF environment despite the absence of point symmetry (or pseudo-symmetry) that would be needed for a strictly axial CF. The off-diagonal elements of the CF play some role and, in the higher-lying doublets of the ground multiplet, the axial nature of the CF is lost (*vide infra*). This demonstrates that strict point symmetry is not required to achieve a highly axial CF, provided the axial parameters are sufficiently strong in comparison to the other CF parameters arising from the low-symmetry components of the CF.

The magnetic relaxation in the Dy-5* cation was studied further by constructing a qualitative relaxation barrier from the *ab initio* results, which follows a methodology in which the transition magnetic moment between the different states was calculated and the relaxation pathway follows the largest matrix elements (Fig. 4B, table S14) (*35*). The results predict that the barrier is crossed at the fourth excited doublet, corresponding to a U_{eff} value of 1,524 cm^{-1} for the Orbach process, which is consistent with the calculated ***g***-tensors for this doublet and is in excellent agreement with the experimentally determined barrier height of 1,541(11) cm^{-1}. To gain deeper insight into the nature of the spin-phonon relaxation, the first-order spin-phonon couplings with the optical phonons (approximated as the molecular vibrations) were evaluated from first-principles calculations (tables S15-S18). In earlier work on $[(Cp^{ttt})_2Dy]^+$ (*14*), vibrations of the C–H oscillators in the Cp rings were recognized as the most important contribution to the Orbach relaxation as they initiated the transition from the ground doublet to the first excited doublet. In the case of Dy-5*, these oscillators are absent, and the analogous transition from the ground to the first excited doublet is most likely initiated by out-of-plane vibrations of the Cp^* ligand when comparing the frequency of these modes (632.9 cm^{-1} and 640.5 cm^{-1}) to the calculated gap between the ground and first-excited doublets (672 cm^{-1}) (see Movies S1-S7). Because the out-of-plane vibrations couple strongly to vibrations of the Cp^* methyl groups, it is conceivable that their energies can be tuned by choosing ligand substituents that would bring the vibrational modes out of resonance with the excitation gap. Such an approach should lead to further improvements in SMM performance beyond those of the Dy-5* cation, and therefore enhance their potential for applications in magnetic information storage materials.

References and Notes:

1. N. Ishikawa, M. Sugita, T. Ishikawa, S. Koshihara, Y. Kaizu, *J. Am. Chem. Soc.* **125**, 8694 (2003).
2. B. M. Day, F.-S. Guo, R. A. Layfield *Acc. Chem. Res*. **51**, 1880 (2018).
3. J.-L. Liu, Y.-C. Chen, M.-L. Tong, *Chem. Soc. Rev*. **7**, 2431 (2018).
4. J. M. Frost, K. L. M. Harriman, M. Murugesu, *Chem. Sci*. **7**, 2470 (2016).
5. M. Shiddiq, D. Komijani, Y. Duan, A. Gaita-Ariño, E. Coronado, S. Hill, *Nature* **531**, 348 (2016)
6. S. Thiele, F. Balestro, R. Ballou, S. Klyatskaya, M. Ruben, W. Wernsdorfer, *Science* **344**, 1135 (2014)
7. D. N. Woodruff, R. E. P. Winpenny, R. A. Layfield. *Chem. Rev*. **113**, 5110 (2013).
8. P. Zhang, L. Zhang, J. Tang, *Dalton Trans*. **44**, 3923 (2015).
9. J. D. Rinehart, M. Fang, W. J. Evans J. R. Long, *J. Am. Chem. Soc.* **133**, 14236 (2011).
10. Y.-C. Chen, J.-L. Liu, L. Ungur, J. Liu, Q.-W. Li, L.-F. Wang, Z.-P. Ni, L. F. Chibotaru, X.-M. Chen, M.-L. Tong, *J. Am. Chem. Soc.* **138**, 2829 (2016).
11. S. K. Gupta, T. Rajeshkumar, G. Rajaraman, R. Murugavel, *Chem. Sci*. **7**, 5181 (2016).
12. F. Liu, D. S. Krylov, L. Spree, S. M. Avdoshenko, N. A. Samoylova, M. Rosenkranz, A. Kostanyan, T. Greber, A. U. B. Wolter, B. Büchner, A. A. Popov, *Nat. Commun*. **8**, 16098 (2017).
13. F.-S. Guo, B. M. Day, Y.-C. Chen, M.-L. Tong, A. Mansikkamäki, R. A. Layfield, *Angew. Chem. Int. Ed*. **56**, 11445 (2017).
14. C. A. P. Goodwin, F. Ortu, D. Reta, N. F. Chilton, D. P. Mills, *Nature* **548**, 439 (2017).
15. C. A. P. Goodwin, D. Reta, F. Ortu, N. F. Chilton, D. P. Mills, *J. Am. Chem. Soc.* **139**, 18714 (2017).
16. S. J. Connelly, W. Kaminsky, D. M. Heinekey, *Organometallics* **32**, 7478 (2013).
17. C. Benelli, D. Gatteschi, *Introduction to Molecular Magnetism: From Transition Metals to Lanthanides*, Wiley-VCH, Weinheim, 2015.
18. Y.-N. Guo, G.-F. Xu, Y. Guo, J. Tang, *Dalton Trans*. **40**, 9953 (2011).
19. S. Demir, M. I. Gonzalez, L. E. Darago, W. J. Evans, J. R. Long, *Nat. Commun*. **8**, 2144 (2017).
20. L. Ungur, L. F. Chibotaru, *Inorg. Chem*. **55**, 10043 (2016).
21. L. Ungur, J. J. Le Roy, I. Korobkov, M. Murugesu, *Angew. Chem. Int. Ed*. **53**, 4413 (2014).
22. J. J. Le Roy, L. Ungur, I. Korobkov, L. F. Chibotaru, M. Murugesu, *J. Am. Chem. Soc*. **136**, 8003 (2014).
23. J. J. Le Roy, M. Jeletic, S. I. Gorelsky, I. Korobkov, L. Ungur, L. F. Chibotaru, M. Murugesu, *J. Am. Chem. Soc*. **135**, 3502 (2013).
24. K. L. M. Harriman, J. J. Le Roy, L. Ungur, R. Holmberg, I. Korobkov, M. Murugesu, *Chem. Sci*. **8**, 231 (2017).
25. T. P. Latendresse, N. S. Bhuvanesh, M. Nippe, *J. Am. Chem. Soc*. **139**, 14877 (2017).
26. T. Pugh, N. F. Chilton, R. A. Layfield, *Angew. Chem. Int. Ed*. **55**, 11082 (2016).
27. T. Pugh, F. Tuna, L. Ungur, D. Collison, E. J. L. McInnes, L. F. Chibotaru, R. A. Layfield, *Nat. Commun*. **6**, 7492 (2015).
28. T. Pugh, V. Vieru, L. F. Chibotaru, R. A. Layfield, *Chem. Sci*. **7**, 2128 (2016).
29. T. Pugh, N. F. Chilton, R. A. Layfield, *Chem. Sci*. **8**, 2073 (2017).
30. A. F. R. Kilpatrick, F.-S. Guo, B. M. Day, A. Mansikkamäki, R. A. Layfield F. G. N. Cloke, *Chem. Commun*. **54**, 7085 (2018).

31. L. Ungur, L. F. Chibotaru, *Computational Modelling of Magnetic Properties of Lanthanide Compounds in Lanthanide and Actinides* in *Molecular Magnetism*. R. A. Layfield, M. Murugesu (Eds,. Wiley-VCH, Weinheim, Germany, 2015.
32. T. Shiozaki, W. Gyõrffy, P. Celani, H.-J. Werner. *J. Chem. Phys*. **135**, 081106 (2011).
33. L. Ungur, L. F. Chibotaru. *Chem. Eur. J.* **23**, 3708 (2017).
34. L. F. Chibotaru in *Advances in Chemical Physics*, *Ab initio Methodology for Pseudospin Hamiltonians of Anisotropic Magnetic Complexes*, Vol. 153 (Eds.: S. A. Rice, A. R. Dinner), Wiley, New York, **2013**, pp. 397–519.
35. L. Ungur, M. Thewissen, J.-P. Costes, W. Wernsdorfer, L. F. Chibotaru, *Inorg. Chem.* **52**, 6328 (2013).

Acknowledgments: The authors thank the CSC-IT Center for Science in Finland, the Finnish Grid and Cloud Infrastructure (persistent identifier urn:nbn:fi:research-infras-2016072533), and Prof. H. M. Tuononen (University of Jyväskylä) for providing computational resources.

Funding: The authors thank the European Research Council (CoG grant 646740), the EPSRC (EP/M022064/1), the NSF China (projects 21620102002, 91422302), the National Key Research and Development Program of China (2018YFA0306001) and the Academy of Finland (projects 282499, 289172).

Author contributions: R.A.L. conceived the original idea and formulated the research aims. Synthetic and crystallographic work was carried out by F.-S.G. and B.M.D. Magnetic measurements were conducted by Y.-C.C. and M.-L.T. The theoretical analysis was carried out by A.M. All authors analyzed the data. R.A.L. wrote the manuscript, with contributions from all authors.

Competing interests: The authors declare no competing interests.

Data and materials availability: Metrical data for the solid-state structures of **1**-**3** are available free of charge from the Cambridge Crystallographic Data Centre under reference numbers CCDC 1854466-1854468. All other data are in the main text supplementary materials.